Dynamic Properties And Microstructural Mechanisms Of Nanoclay-modified Cement-stabilized Soil

Xinshan Zhuang*, Yuhan Hao, Duan Yang, and Zhuona Chen

School of Civil Engineering, Architecture and Environment, Hubei University of Technology, Wuhan 430068, Hubei Province, China

** Corresponding author. E-mail: zhuangxinshan@hbut.edu.cn*

Received: Aug. 26, 2025; Accepted: Mar. 05, 2026

To address serviceability issues of railway subgrades in Central China subjected to dynamic loading, this study investigated the dynamic behavior and microstructural mechanisms of nanoclay-modified, cement-stabilized silty clay. Specimens with var-ying nanoclay contents were prepared and tested using a dynamic triaxial apparatus, and cumulative plastic strain and dynamic elastic modulus were measured. Micro-structural and mineralogical characteristics were examined by scanning electron mi-croscopy and X-ray diffraction. The results showed that cumulative plastic strain increased with dynamic stress amplitude, whereas dynamic elastic modulus decreased. By contrast, increasing nanoclay content reduced cumulative plastic strain and increased dynamic elastic modulus, with 0.5% identified as the optimum content; beyond 0.5%, the marginal benefit diminished. Relative to cement-stabilized soil without nanoclay, cumulative plastic strain decreased by approximately $35-50\%$, while dynamic elastic modulus increased by about $75-82\%$. Microstructurally, nanoclay promoted the formation of $C-(A)-S-H$, reduced pore space, and densified the interfacial transition zone. These findings elucidate the governing trends in the dynamic response of nanoclay-modified silty clay and provide a basis for the design of nanoclay-modified railway subgrades in Central China.

Keywords: Nanoclay; Silty clay; Cumulative plastic strain; Dynamic elastic modulus; Dynamic triaxial test; Microstructural mechanisms

http://dx.doi.org/10.6180/jase.202609_32.005

1. Introduction

In Central China, silty clay is widely distributed, and the rapid regional development and large-scale transportation projects have made silty-clay foundations an unavoida-ble engineering concern. Such foundations are characterized by low bearing capacity, high moisture sensitivity, poor compactability, and a tendency toward liquefaction under dynamic loading. Under long-term vehicular loads, silty-clay subgrades are prone to cumulative deformation and substantial lateral displacement. To mitigate these issues, lime or cement has commonly been used to stabilize the soil. Long-term field evaluations by Das et al. [1] and laboratory tests by Shi et al. [2] demonstrated that lime significantly improved the mechanical and shear properties of silty clay, with performance dependent on dosage. Cement stabilization also increased soil strength, with efficacy influenced by curing time and temperature. However, the production of these traditional binders consumes large amounts of natural resources and emits sub-stantial pollutants, which conflicts with China's carbon-neutral strategy; moreover, cement- and lime-stabilized soils often exhibit increased brittleness and cracking [3, 4]. Consequently, there is an urgent need for stabilization materials that are both low-carbon and reliable in service.

Nanomaterials and nanotechnology have been hailed as among the most promising developments of the twenty-first century. With advances in nanotechnology, research

on the application of nanomaterials to improve cement-stabilized soils has deepened, wherein nano-silica (SiO_2) [5, 6], nano-alumina (Al_2O_3) [7, 8], nano-titania (TiO_2) [9], nano-zinc oxide (ZnO) [10], nano-calcium carbonate ($CaCO_3$) [11], and carbon nano-tubes (CNTs) [12] have been incorporated as supplementary nano-admixtures to par-tially replace cement.

Owing to its high specific surface area and layered microstructure, nanoclay has been regarded as a particularly promising nano-modifier. Zoriyeh et al. reported that an appropriate nanoclay dosage filled micropores, reduced cracking, and enhanced the strength and durability of highly plastic fine-grained soils [13]. Using resonant column tests, Ochoa-Cornejo et al. showed that adding 1% nanoclay to sand increased smallstrain shear stiffness across confining pressures, with stiffness continuing to rise with longer consolidation times [14]. Kananizadeh et al. [15] further demonstrated that nanoclay markedly lowered the hydraulic conductivity of clays and improved their swelling resistance, while Abbasi et al. observed reductions in dispersivity and erosion susceptibility, thereby improving engineering stability [16]. Although these studies have highlighted the advantages of nanoclay in terms of static properties, permeability, and small-strain behavior, comparatively little work has examined nanoclay-modified, ce-ment-stabilized silty clay under dynamic loading. In particular, systematic investigations into dynamic elastic modulus, cumulative plastic strain, and the associated microstructural mechanisms remain limited.

To this end, a series of tests was conducted on nanoclay-modified, ce-ment-stabilized silty clay to systematically examine how nanoclay content and dy-namic stress amplitude affected cumulative plastic strain and dynamic elastic modulus. The modification mechanisms were elucidated through scanning electron microscopy (SEM) and X-ray diffraction (XRD) analyses. The results substantiate the mechanistic role of nanoclay in improving soil behavior and provide a theoretical basis for its ap-plication to railway subgrades.

2. Materials and methods

2.1. Materials

The silty clay used in this study was sampled from Wuhan, Hubei Province, China (Fig. 2(a)). Compaction tests determined a maximum dry density of 1.63 g/cm^3 and an optimum water content of 17%. The soil's basic index properties are summarized in Table 1. The particle-size distribution was obtained from combined sieve and hydrometer analyses; the resulting gradation curve is shown in Fig. 1.

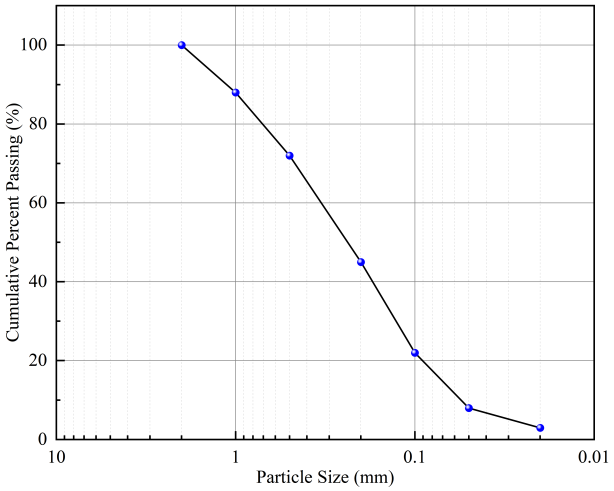

Fig. 1. Gradation curve of silty clay.

Nanoclay is a layered aluminosilicate nanomaterial dominated by montmorillo-nite and characterized by a plate-like morphology. It was supplied as a white powder (Fig. 2(b)). The product used in this study was manufactured by Yicheng Jingrui New Materials Co., Ltd., Anhui Province, China, and its principal chemical composition is summarized in Table 2.

The cement used in this study was P.O 42.5 ordinary Portland cement. It was supplied as a gray powder (Fig. 2(c)). The cement was provided by a building materials company in Anhui Province, China, and its principal chemical composition is listed in Table 3.

2.2. Specimen Preparation

The silty clay was air-dried, crushed, and passed through a 2 mm sieve; the passing fraction was oven-dried at 105°C for 24 h [17]. A prescribed mass ratio of cement and nanoclay was then blended uniformly into the dried soil. Deionized water was added at the previously determined optimum water content and thoroughly mixed; specimens were molded within 60 min of mixing. Cylindrical specimens were prepared by layered compaction in five lifts, each compacted to the target height. After each lift, the surface was lightly scarified to a depth of about 1 mm to enhance interlayer bonding [18]. The finished specimens measured 50 mm in diameter and 100 mm in height. After molding, the specimens were kept in the molds for 24 h , then demolded, wrapped in plastic film, and cured for 28 d in a temperature-humidity chamber at 23 $\pm$ 2°C and relative humidity > 95%.

Table 1. Basic physical properties of silty clay.

Max dry density ρd/ $(g \cdot cm^{-3})$	Optimum water content w_{opt} /%	Liquid limit W_L/%	Plastic limit W_P/%	Plasticity index I_P/%
1.63	17.0	29	21	8

Table 2. BChemical composition of nanoclay (w_t.%).

SiO_2	Al_2O_3	MgO	CaO	Na_2O	Fe_2O_3	K_2O	Others
60.5	18.2	3.8	1.5	2.0	3.5	0.5	10

Table 3. Chemical composition content of cement (w_t.%).

CaO	SiO_2	Fe_2O_3	Al_2O_3	MgO	K_2O	SO_3	Others
59.27	23.15	3.23	6.13	2.24	0.87	3.91	1.2

(a) Silty cla. (b) Nanoclay. (c) Cement.

Fig. 2. Test materials.

2.3. Methods

2.3.1. Dynamic Triaxial Tests

The dynamic triaxial testing system (GDS Instruments, UK; Fig. 3) comprised a pressure cell, confining pressure control, and back-pressure control modules. The maximum confining pressure capacity was 2 MPa , and the loading frequency ranged from 0.001 to 5 Hz . The system was fully automated via GDSLAB software, enabling precise application of axial load, confining pressure, and back pressure; with a displacement-control resolution of 0.0001 mm . Pore water pressure, volumetric strain, and axial strain were recorded in real time. The apparatus provides both static and dynamic loading modes; in this study, the dynamic module was used to apply dynamic axial loading to the specimens. Specimens were first vacuum-saturated and then saturated using the back-pressure method. The degree of saturation was verified by measuring the pore-water pressure coefficient (B); when B exceeded 0.95, the specimen was considered fully saturated.

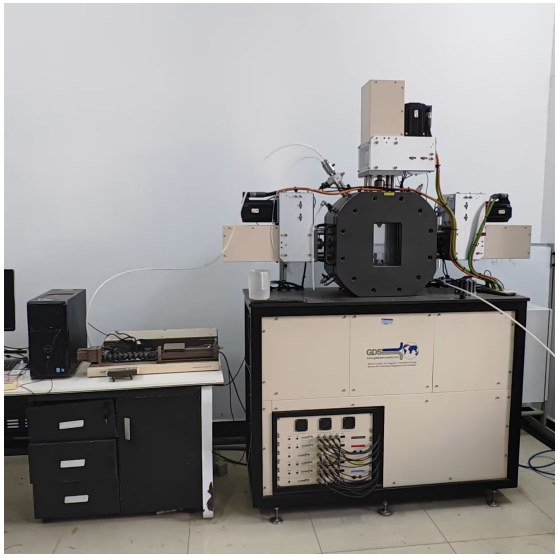

Fig. 3. GDS dynamic triaxial testing system.

Previous studies indicated that the confining pressure in the shallow subgrade bed layer was approximately $25-60$kPa; for trains with axle loads of 19.6-22.5 t, the corresponding dynamic stress amplitude reached about $32-185$kPa [19]. In Central China, the predominant freight car type is the C70E, with a maximum payload of 70 t and

a tare weight of 24t [20]. To examine the bearing capacity of improved silty-clay subgrades under high service loads, dynamic stress amplitudes of 50, 100, 150, and 200 kPa were adopted. A confining pressure of 40 kPa was applied to represent shallow subgrade conditions. In accordance with prior studies, a sinusoidal waveform is appropriate for consolidated-undrained testing [21], as illustrated in Fig. 4. During the dynamic stage, each specimen was subjected to 10,000 cycles at a fixed frequency. Based on the design speed of the C70E ($v = 33$ m/s) and the length of a single car ($l = 13.98$ m), according to Eq. (1), as proposed by Yang et al. [22], the characteristic loading frequency was calculated as $f \approx 2$ Hz; this value was adopted as the representative dominant frequency for cyclic loading in the present tests.

$$f = \frac{v}{l} \tag{1}$$

Prior studies indicated that, to mitigate particle agglomeration and maintain specimen workability, the nanoclay content should be kept below 1% [23]. In addition, a cement content of 5% was sufficient to meet basic bearing-capacity requirements while helping control material costs [24]. Accordingly, this study adopted nanoclay contents of $0, 0.25, 0.5, 0.75$, and 1.0% (by dry mass of soil), with the cement content fixed at 5%, and a curing period of 28 days, which is commonly adopted to represent the shortto medium-term strength development of cement-stabilized soils. Three specimen groups were prepared: natural soil; a cement-stabilized control (5% cement, 0% nanoclay); and nanoclay-modified soils (5% cement with $0.25 - 1.0$% nanoclay). The dynamic triaxial testing matrix is summarized in Table 4.

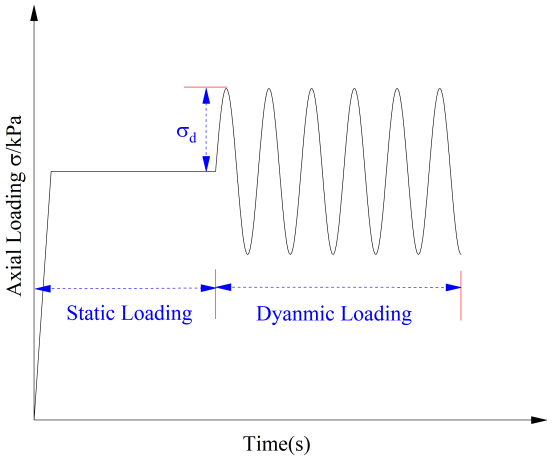

Fig. 4. Schematic of a sine wave.

2.3.2. *Scanning Electron Microscopy (SEM)*

SEM observations were conducted using a SIGMA high-resolution field-emission scanning electron microscope (Carl Zeiss, Germany). The system comprised electron-optics, signal acquisition and processing, imaging/recording, vacuum, and power/control subsystems. Secondary-electron images acquired at an accelerating voltage of 15 kV achieved nominal nanometer-scale resolution, and all micrographs include scale bars. After completion of the dynamic triaxial tests, subsamples were taken from the axial mid-height of the specimens to examine the pore structure of the cement-stabilized soil and features at particle interfaces.

2.3.3. *X-ray Diffraction (XRD)*

X-ray diffraction tests were performed using an Empyrean diffractometer (PANalytical, Netherlands). Scans were conducted over $2\theta = 10^\circ - 80^\circ$ with a step size 0.02° and a scan rate of 10°/min. The diffraction patterns were processed with Jade 6.5, and phase identification and semi-quantitative assessment of the principal minerals were carried out with reference to the ICDD PDF-4+ database.

3. Results and discussion

3.1. Evolution of Cumulative Plastic Strain

Cumulative plastic strain (ε_p) refers to the strain accumulation in soils under dynamic loading arising from interparticle slip and structural reorganization. It reflects the plastic deformation process and is strongly influenced by confining pressure, water content, dynamic stress amplitude, and relative compaction [25]. In this study, the natural soil specimen subjected to $\sigma_d = 200$kPa exhibited a rapid ε_p increase to about 10% after 1,000 cycles, indicating pronounced failure. Accordingly, subsequent analyses of ε_p and dynamic elastic modulus focus on the cement-stabilized and nanoclay-modified soils; subsequent comparisons involving the natural soil are confined to the microstructural section. For brevity, only representative datasets are presented herein.

3.1.1. *Effect of Dynamic Stress Amplitude*

Fig. 5 plots the evolution of cumulative plastic strain with the number of cycles for different dynamic stress amplitudes. The ε_p increased with increasing amplitude. Taking the cement-stabilized control (5% cement, 0% nanoclay) at a confining pressure of 40 kPa and $N = 10,000$ cycles as the reference, the final ε_p at amplitudes of 100,150 , and 200 kPa was higher by approximately 73%, 136%, and 225%, respectively (relative to 50 kPa). In addition, at lower amplitudes ε_p approached a stable value more rapidly, whereas higher

Table 4. Dynamic triaxial test scheme.

Nanoclay content C_{NC}/%	Cement content C_c/%	Dynamic stress amplitude σ_d/kPa	Confining pressure σ_3/kPa	Frequency f/Hz
0,0.25,0.5,	5	50,100,150,	40	2
0.75,1		200		

amplitudes required more cycles to reach stabilization, consistent with previous findings. Under the present test conditions, the curves at all amplitudes became essentially stable after about 4,000 cycles.

Mechanistically, a higher dynamic stress amplitude imposes greater dynamic shear, repeatedly weakening interfacial bonds. The ensuing stiffness degradation and pore-structure reorganization reduce the soil's load-bearing and recovery capacity over subsequent cycles, thereby accelerating plastic strain accumulation. Hence, in-creasing amplitude amplifies the plastic strain demand a key reason that high-amplitude loading should be carefully controlled.

3.1.2. Effect of Nanoclay Content

Fig. 6 shows the relationship between nanoclay content and ε_p at various dynamic stress amplitudes. The final ε_p increased monotonically with amplitude, while the datasets at each amplitude were clearly stratified by nanoclay content: the 0% group remained the highest throughout, whereas 0.5% produced the lowest ε_p. Relative to the cement-stabilized control without nanoclay, the final ε_p was reduced by approximately $20-40\%$ at 0.25% nanoclay, $35-50\%$ at $0.5\%, 10-25\%$ at 0.75%, and $15-30\%$ at 1.0%. At lower amplitudes the intergroup differences were modest, but the gaps widened with increasing amplitude; across all amplitudes, specimens with nanoclay exhibited lower ε_p than the unamended control, with 0.5% emerging as the optimal content. When the nanoclay content exceeded $0.75-1.0\%$, the incremental reduction in ε_p became marginal, indicating diminishing returns likely associated with particle agglomeration and less effective dispersion.

The above results indicate that adding nanoclay effectively suppresses cumulative plastic deformation. Mechanistically, owing to its small particle size and high specific surface area, nanoclay fills micropores within the soil skeleton, regulates interfacial water films and pore-water distribution, maintains a favorable local hydration environment, and promotes the nucleation and growth of $C-(A)-S-H$. These processes densify particle-binder interfaces and enhance structural continuity. By contrast, excessive nanoclay tends to agglomerate, increasing the effective particle size, reducing available surface area, and weakening interparticle interfaces. Overdosage also competes for free water, impeding cement hydration and diminishing effective interparticle contact, which ultimately increases cumulative plastic strain.

3.2. Analysis of Dynamic Elastic Modulus

The dynamic elastic modulus (E_d) is defined as the ratio of dynamic stress to the recoverable component of dynamic strain, describing the elastic response of soil under dynamic loading [26]. The corresponding definition is given in Eq. (2). During the loading stage of each dynamic triaxial test, a stress-strain hysteresis loop was generated in every cycle. For a given cycle, the E_d was taken as the secant slope of the line connecting the two peak points on the loop, i.e.

$$E_d = \frac{\sigma_{d,max} - \sigma_{d,min}}{\varepsilon_{d,max} - \varepsilon_{d,min}} \tag{2}$$

In this formulation, $\sigma_{d,\,max}$, $\sigma_{d,\,min}$ and $\varepsilon_{d,\,max}$, $\varepsilon_{d,\,min}$ denote the maximum and minimum dynamic stresses and strains within a given loading cycle. In this study, σ_d and ε_d, were extracted using a stratified sampling schedule: for $N \leqq 10$, one hysteresis loop was sampled every cycle; for $10 < N \leqq 100$, one loop every 10 cycles; for $100 < N < 1000$, one loop every 100 cycles; and for $N \geqq 1000$, every 1000 cycles, where N is the cumulative number of cycles.

3.2.1. Effect of Dynamic Stress Amplitude

Fig. 7 presents the relationships between dynamic elastic modulus and dynamic strain at different dynamic stress amplitudes.As σ_d increases, the dynamic elastic modulus exhibits an overall downward trend. For a given number of cycles, the E_d decreases progressively with increasing σ_d, and the reduction is more pronounced at higher amplitudes. Using $\sigma_d = 50$kPa as the baseline, increasing σ_d to 100, 150, and 200 kPa reduced E_d by approximately $3.9-12.8\%, 7.4-15.9\%$, and $10.9-25.6\%$, respectively. This sustained loss of dynamic stiffness with amplitude indicates stronger nonlinearity and cumulative damage at higher stress levels.

With respect to the magnitude of dynamic strain, the evolution of E_d can be divided into three regimes. At small dynamic strains, the response is essentially elastic and E_d remains nearly constant. As dynamic strain increases, E_d declines rapidly toward a threshold dynamic strain, plastic strain begins to accumulate, and the soil transitions from

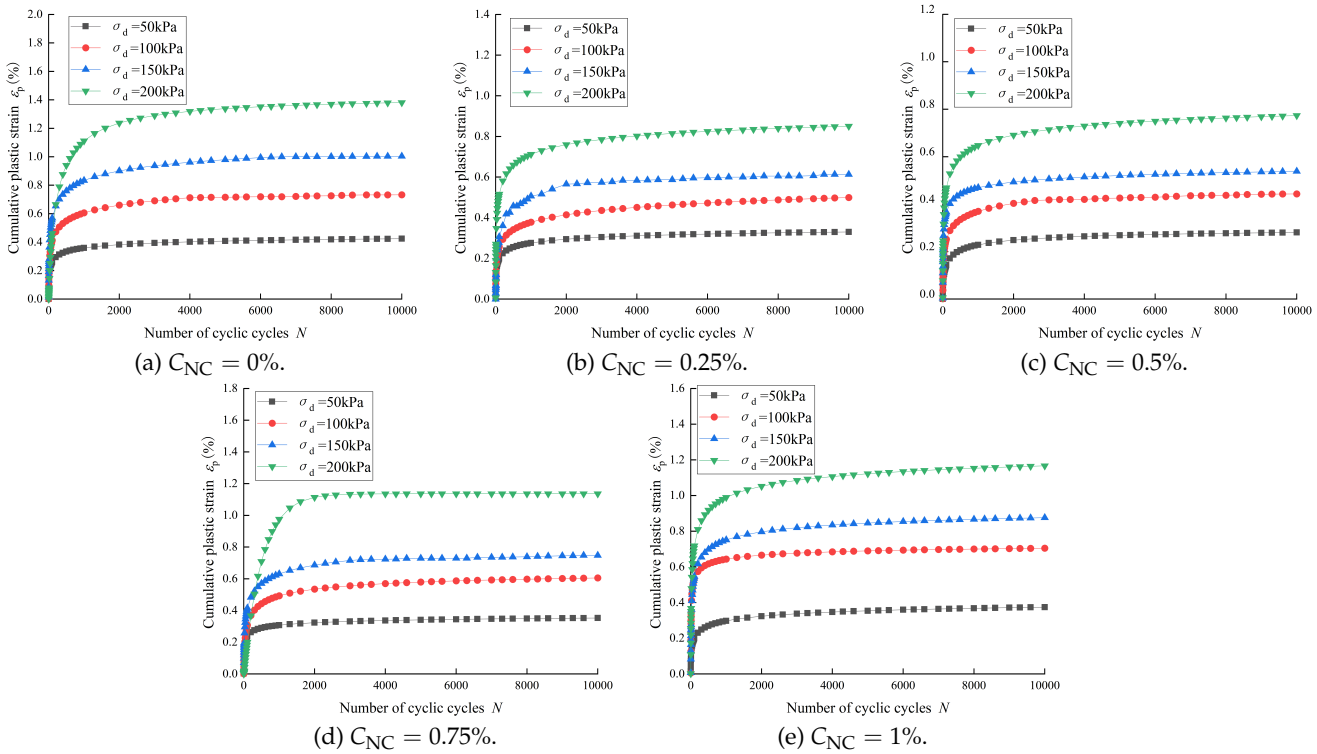

(a) $C_{NC} = 0\%$. (b) $C_{NC} = 0.25\%$. (c) $C_{NC} = 0.5\%$.

(d) $C_{NC} = 0.75\%$. (e) $C_{NC} = 1\%$.

Fig. 5. Cumulative plastic strain versus number of loading cycles under different dynamic stress amplitudes.

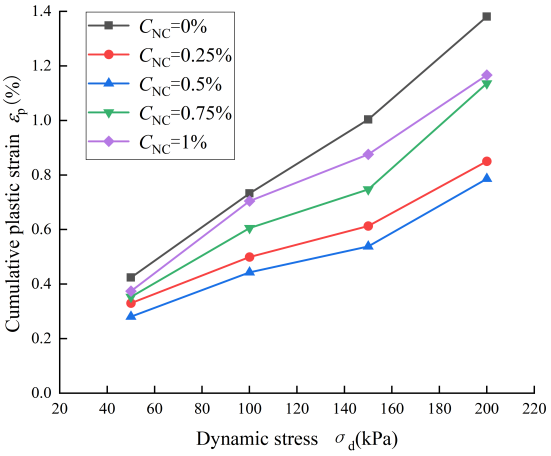

Fig. 6. Curve of nanoclay content versus cumulative plastic strain.

an elastic to an elasto-plastic state. With further increase in dynamic strain, the rate of reduction in E_d diminishes and the curve gradually flattens, indicating that the recoverable component becomes minor and the response is dominated by plastic deformation.

3.2.2. *Effect of Nanoclay Content*

Fig. 8 shows the relationship between nanoclay content and dynamic elastic modulus. Incorporating nanoclay markedly increased the modulus relative to the cement-stabilized control without nanoclay: about $35-40\%$ at 0.25%, $75-82\%$ at 0.5%, $10-24\%$ at 0.75%, and $10-14\%$ at 1.0%. The content effect exhibits a rise-then-decline pattern: although the peak modulus continues to increase with added nanoclay, the incremental gain diminishes beyond approximately $0.5-0.75\%$. Overall, 0.5% is identified as the optimal content under the present test conditions.

Mechanistically, an appropriate amount of nanoclay fills micropores, regulates interfacial water films, and promotes the formation of $C-(A)-S-H$, thereby making the soil skeleton more continuous and stiffer. By contrast, excessive nanoclay tends to agglomerate and sequester water needed for cement hydration, generating locally weakly cemented regions and macrovoids, which in turn lowers the dynamic elastic modulus.

3.3. SEM Analysis

To elucidate the microstructure of nanoclay-modified soils at different contents, scan-ning electron microscopy was performed, with natural soil and cement-stabilized soil serving as controls. Fig. 9 presents SEM micrographs of cement-stabilized silty clay at varying nanoclay contents.

Fig. 9(a) shows SEM images of the natural soil at 1000× and 500× magnifica-tion. The fabric was dominated by loosely packed, plate-like particles with predomi-nantly

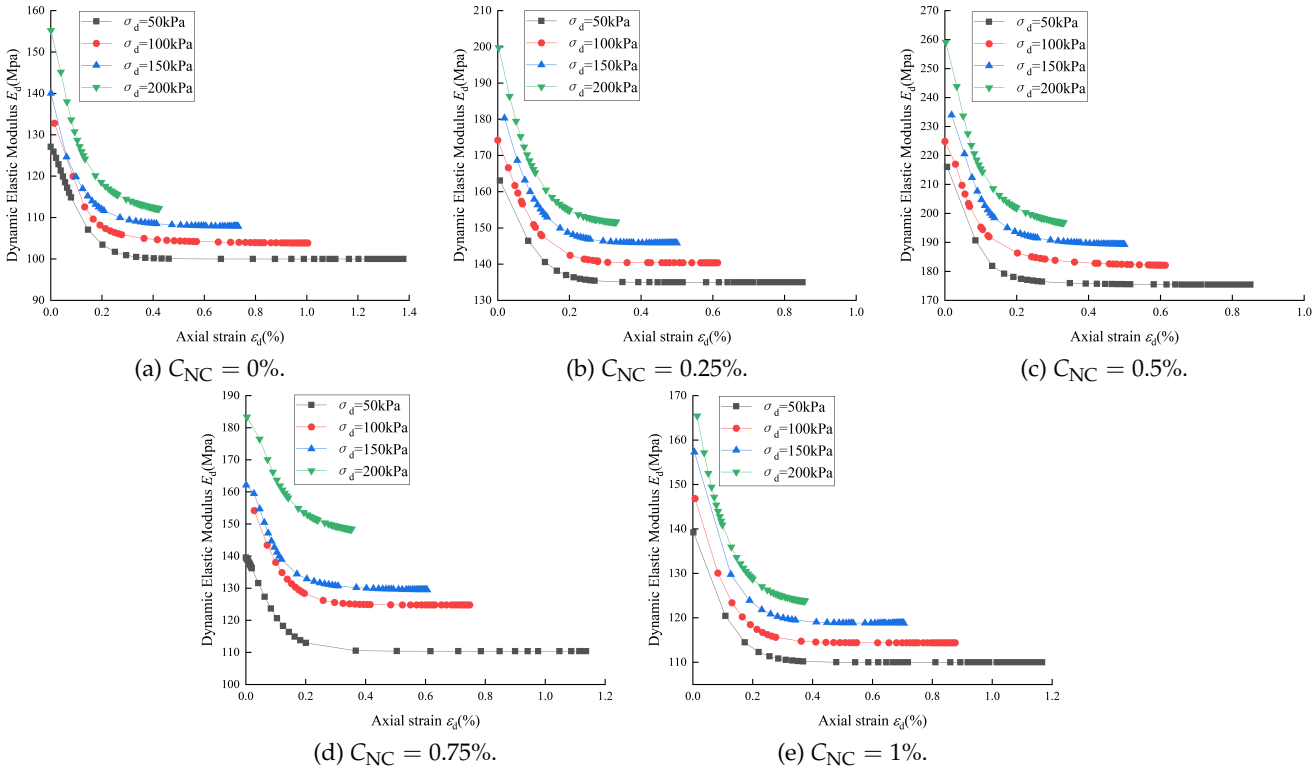

(a) $C_{NC} = 0\%$. (b) $C_{NC} = 0.25\%$. (c) $C_{NC} = 0.5\%$.

(d) $C_{NC} = 0.75\%$. (e) $C_{NC} = 1\%$.

Fig. 7. Dynamic elastic modulus versus dynamic strain under different dynamic stress amplitudes.

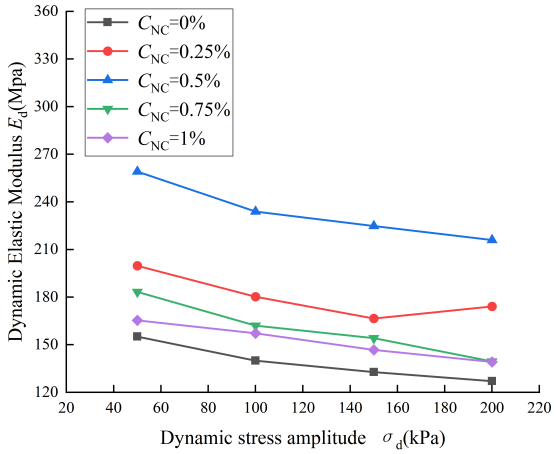

Fig. 8. Relationship between nanoclay content and dynamic elastic modulus.

point contacts and a highly connected pore network. Local lamellar exfoliation and weak interparticle interfaces were evident. Overall, the skeleton exhibited a loose and porous character, lacking a continuous cemented matrix, and was therefore prone to structural reorganization and pore collapse under dynamic loading.

Fig. 9(b) shows SEM micrographs of the cement-stabilized soil at 500× and 2000× magnification. Compared with the natural soil, hydration products ($C-S-H$) partially enveloped soil grains and formed interparticle bridges, the interfacial transition zone became relatively dense, and pore connectivity decreased markedly. At higher magnification, pore walls appeared more continuous, with lamellae/floccules "stitched" by the gel phase, indicating that hydration established load-transfer paths across parti-cles. Nonetheless, the gel network remained locally discontinuous, and some pores were relatively large, suggesting incomplete and nonuniform coverage of the particle surfaces.

Fig. 9(c) presents SEM micrographs of the nanoclay-modified cement-stabilized soil at 500× and 2000× magnification. Following nanoclay incorporation, a denser cementitious matrix was observed: $C-S-H$ was more continuously distributed on particle surfaces and within pores, the interfacial transition zone became clearer with a more uniform thickness, and pore connectivity was further reduced. At 2000×, interparticle voids were effectively infilled by cementitious products, agglomeration appeared controlled, and few indications of microcracking were present.

SEM observations indicated that the natural soil was characterized by loose flocculated packing and highly connected pores. With cement addition, hydration products (C-S-H) formed interparticle bridges, the interfacial transi-

tion zone densified, and pore connectivity decreased. Incorporating 0.5% nanoclay further increased the coverage and continuity of the gel phase, refined the pore structure, and improved the uniformity of the interfacial transition zone. Taken together, nanoclay-modified cement-stabilized soil generated a greater amount of more continuous $C-S-H$, enhancing the integrity of the microstructural framework and the continuity of load-transfer paths. This microstructural evidence underpins the observed reduction in cumulative plastic strain, the increase in dynamic elastic modulus, and the improvement in dynamic stability at the macroscale.

3.4. XRD Analysis

To elucidate the role of nanoclay in cement-stabilized soil, X-ray diffraction was per-formed on the natural soil, the cement-stabilized soil, and the nanoclay-modified soil for qualitative phase identification and comparison of crystal-structure evolution; the results are shown in Fig. 10.

In the natural soil, the dominant diffraction peaks corresponded to quartz, yield-ing a typical siliceous-soil pattern. This indicates a mineral assemblage composed chiefly of stable aluminosilicate minerals; no hydration products or other cementitious phases were detected, implying a microstructure governed by physical packing with little chemical cementation.

In the cement-stabilized specimen, in addition to quartz, several crystalline phases produced by cement hydration were clearly observed. Pronounced reflections of portlandite ($Ca(OH)_2$) confirmed active hydration. Peaks attributable to ettringite were also present, indicating early formation of AFt phases that contribute to initial strength development. In addition, calcite was identified, likely formed by carbonation of portlandite through reaction with atmospheric CO_2. Notably, a broad amorphous hump appeared in the mid-2 θ range, characteristic of calcium-silicate-hydrate ($C-S-H$) gel. As the principal binding phase of cement hydration, the amount and spatial distribution of C-S-H exert a decisive influence on the strength and stability of the soil matrix.

In the nanoclay-modified specimen, the crystalline phases were broadly consistent with those in the cement-stabilized soil. A more pronounced amorphous hump together with clearer $C-(A)-S-H$ features indicates that nanoclay facilitates gel nucleation and structural development and improves the reaction efficiency at paste-soil interfaces. Peak intensities of crystalline hydrates (e.g., ettringite and portlandite) increased in the early stage, consistent with accelerated hydration via adsorption and interfacial activation; with curing, partial consumption of portlandite by pozzolanic reactions further strengthens the amorphous background. No additional reflections were detected, implying that nanoclay acts mainly as a reaction promoter and structural regulator rather than introducing new crystalline phases.

XRD results indicate that the natural soil lacks intrinsic cementation, whereas cement stabilization effectively introduces hydration products that build a load-bearing skeleton and binding network. With the incorporation of nanoclay, the crystalline phase assemblage remains essentially unchanged; however, the amount of $C-(A)-S-H$ gel increases and the amorphous structure becomes more coherent, reflecting enhanced interfacial reaction efficiency between cement paste and soil particles and a denser matrix. Collectively, these changes improve the material's resistance to deformation and its mechanical performance.

3.5. Mechanistic Interpretation

Integrating the microstructural observations and mechanistic considerations. As shown in Fig. 11, a mechanistic model for nanoclay-modified, cement-stabilized silty clay is proposed. The model posits three coupled pathways by which nanoclay enhances per-formance: promotion of cement hydration, participation in pozzolanic reactions, and a filler effect that refines the pore structure and reduces pore connectivity.

Promotion of cement hydration: When nanoclay is incorporated into cement-stabilized silty clay, its primary effect is to accelerate cement hydration, evidenced by increased formation of calcium-silicate-hydrate ($C-S-H$), portlandite ($Ca(OH)_2$), ettringite (AFt) and other hydration products. Representative reactions are:

$$2Ca_3SiO_5 + 6H_2O \rightarrow 3Ca(OH)_2 + 3CaO \cdot 2SiO_2 \cdot 3H_2O$$

$$2Ca_2SiO_4 + 4H_2O \rightarrow Ca(OH)_2 + 3CaO \cdot 2SiO_2 \cdot 3H_2O$$

$$Ca_4Al_2Fe_2O_{10} + 3CaSO_4 2H_2O + 26H_2O \rightarrow$$

$$Ca_6\,(Al, Fe_2)_2\,(SO_4)_3\,(OH)_{12} 26 \cdot H_2O$$

$$Ca_3Al_2O_6 + 3CaSO_4 \cdot 2H_2O + 26H_2O \rightarrow$$

$$Ca_6Al_2\,(SO_4)_3\,(OH)_{12} \cdot 26H_2O$$

Pozzolanic reaction: Owing to its high contents of reactive alumina (Al_2O_3), nanoclay exhibits strong pozzolanic activity and reacts with portlandite ($Ca(OH)_2$) released during cement hydration. These secondary reactions generate additional $C-S-H$ and $C-A-S-H$ gels, reduce the fraction of brittle crystalline phases, refine and densify the gel network, and thereby improve the compactness of the soil matrix. Representative reactions are:

$$Al_2O_3 + 2Ca(OH)_2 + 6H_2O \rightarrow 2CaO \cdot Al_2O_3 \cdot 8H_2O$$

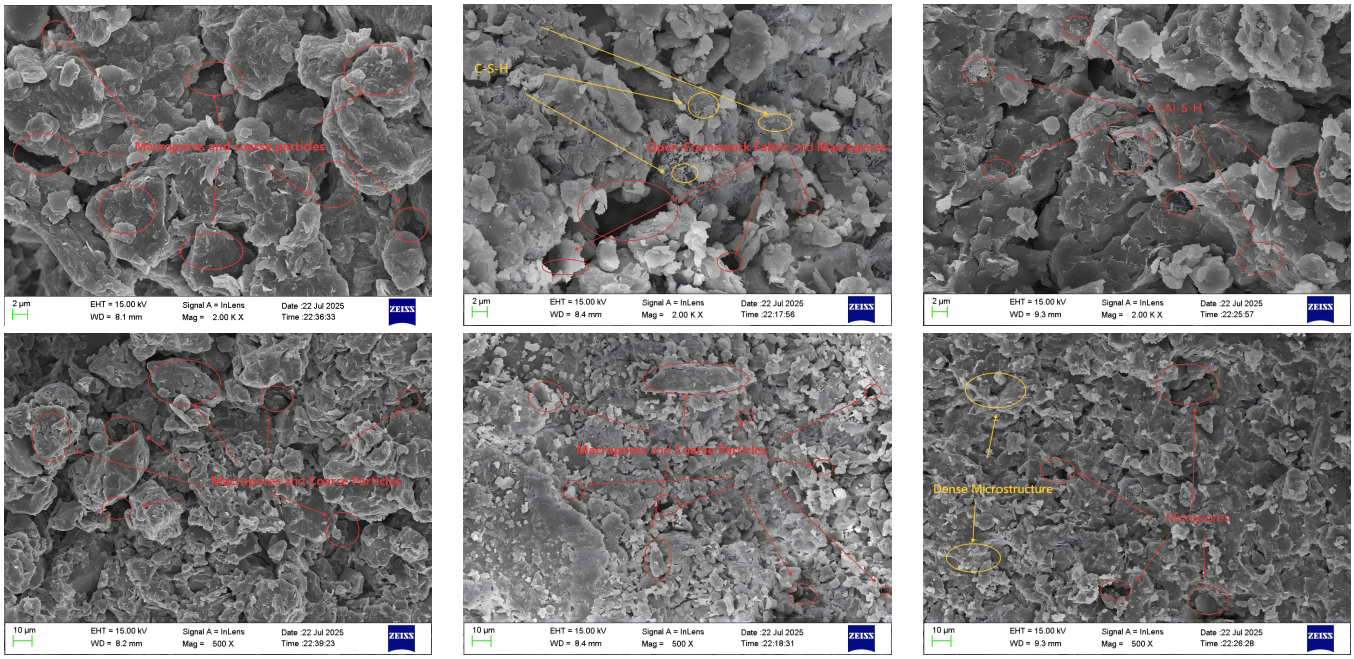

(a) $C_{NC} = 0\%$, $C_C = 0\%$. (b) $C_{NC} = 0\%$, $C_C = 5\%$. (c) $C_{NC} = 0.5\%$, $C_C = 5\%$.

Fig. 9. SEM micrographs of natural soil, cement-stabilized soil and nanoclay-modified soil.

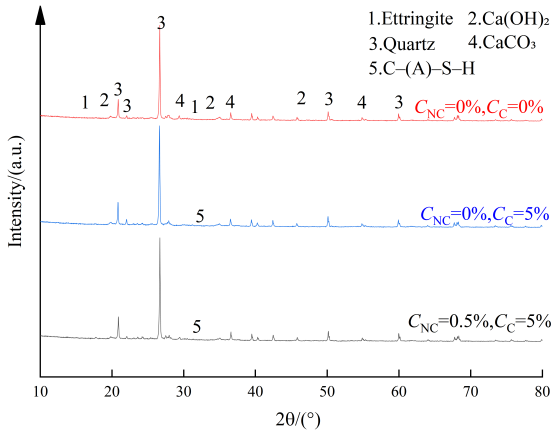

Fig. 10. X-ray diffraction patterns of natural soil, cement-stabilized soil and nanoclay-modified soil.

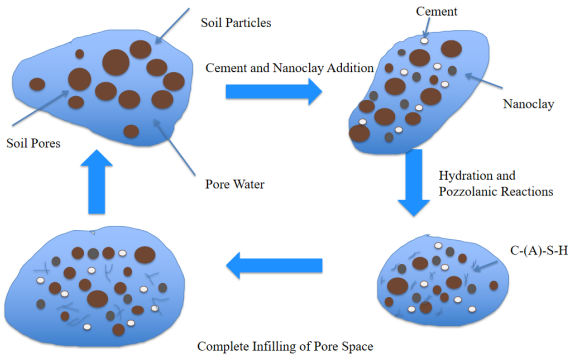

Fig. 11. Mechanistic model for nanoclay–modified cement-stabilized silty clay.

Filler effect: Due to its nanometric particle size and high specific surface area, nanoclay effectively fills macrovoids within the silty-clay skeleton, reducing initial porosity and pore connectivity. This pore-structure refinement facilitates tighter packing of fines during compaction and curing, leading to a denser and more contin-uous matrix.

4. Conclusions

This study employed dynamic triaxial and microstructural tests to investigate the dy-namic behavior and mechanisms of nanoclay-modified, cement-stabilized silty clay. The main conclusions are:

1. The improved subgrade soil is highly sensitive to dynamic stress amplitude. As the amplitude increases, cumulative plastic strain increases monotonically, whereas dy-namic elastic modulus decreases, evidencing the damage effect of high-amplitude loading.

2. Over the investigated range, varying the nanoclay content markedly affects both the cumulative plastic strain and the dynamic elastic modulus of the soil. An addition of 0.5% yields the best overall performance:

relative to the cement-stabilized control without nanoclay, cumulative plastic strain decreases by about $35-50\%$, while dynamic elastic modulus increases by about $75-82\%$. When the content exceeds 0.75%, the improvement diminishes.

3. Microstructural observations show that, compared with natural soil, cement stabilization forms C-S-H gel that fills pores and densifies particle interfaces; the incorporation of nanoclay further refines the pore structure, increases gel coverage and continuity, markedly reduces connected pores, promotes additional C-(A)-S-H formation, and optimizes the cementation network.

4. The enhancement arises from three coupled mechanisms-promotion of hydration, pozzolanic reaction, and a filler effect-which jointly densify the soil skeleton and the interfacial transition zone, thereby suppressing deformation under dynamic loading and increasing dynamic stiffness and stability.

5. Despite the findings presented herein, several limitations should be acknowledged. The experiments were conducted under a constant confining pressure and a single curing condition, and the effects of complex service environments, such as wet–dry cycling, were not considered. The selected confining pressure mainly represents shal-low subgrade conditions, and the behavior under higher confining pressures requires further investigation. In addition, this study focused on cumulative plastic strain and dynamic elastic modulus, while damping characteristics related to energy dissipation were not analyzed. Future work will address these aspects under more diverse service conditions.

Acknowledgements

This study was financially supported by the National Natural Science Foundation of China (Nos. 51978248 and 41772332). This support is gratefully acknowledged.

References

[1] G. Das, A. Razakamanantsoa, G. Herrier, L. Saussaye, D. Lesueur, and D. Deneele, (2021) *"Evaluation of the long-term effect of lime treatment on a silty soil embankment after seven years of atmospheric exposure: Mechanical, physicochemical, and microstructural studies"* **Engineering Geology *281***: 105986. DOI: 10.1016/j.enggeo.2020.105986.

[2] Y. Shi, S. Li, T. Zhang, J. Liu, and J. Zhang, (2024) *"Compaction and shear performance of lime-modified high moisture content silty clay"* **Case Studies in Construction Materials *21***: e03529. DOI: 10.1016/j.cscm.2024.e03529.

[3] G. Rajasekaran, (2005) *"Sulphate attack and ettringite formation in the lime and cement stabilized marine clays"* **Ocean Engineering *32***: 1133–1159. DOI: 10.1016/j.oceaneng.2004.08.012.

[4] Y. Wang, Z. Liu, W. Wan, A. Nie, Y. Zhang, and C. Han, (2023) *"Toughening effect and mechanism of rice straw fiber-reinforced lime soil"* **Construction and Building Materials *393***: 132133. DOI: 10.1016/j.conbuildmat.2023.132133.

[5] S. H. Bahmani, B. B. Huat, A. Asadi, and N. Farzadnia, (2014) *"Stabilization of residual soil using SiO2 nanoparticles and cement"* **Construction and Building Materials *64***: 350–359. DOI: 10.1016/j.conbuildmat.2014.04.086.

[6] N. Ghasabkolaei, A. Janalizadeh, M. Jahanshahi, N. Roshan, and S. Ghasemi, (2016) *"Physical and geotechnical properties of cement-treated clayey soil using silica nanoparticles: An experimental study"* **European Physical Journal Plus *131***: 134. DOI: 10.1140/epjp/i2016-16134-3.

[7] N. Farzadnia, A. A. A. Ali, and R. Demirboga, (2013) *"Characterization of high strength mortars with nano alumina at elevated temperatures"* **Cement and Concrete Research *54***: 43–54. DOI: 10.1016/j.cemconres.2013.08.003.

[8] D. Yang, X. Zhuang, B. Yang, and G. Tao, (2025) *"Dynamic properties and micro-mechanisms of nano-Al2O3 modified cement-stabilized soil under seawater erosion"* **Marine Georesources and Geotechnology *43***: 1948–1961. DOI: 10.1080/1064119X.2024.2445179.

[9] Q. Jili, Z. Yawen, Q. Weiqing, Z. Xiaoshun, H. Lingqing, and C. Jinrui, (2021) *"Nano titanium oxide for modifying water physical property and acid-resistance of alluvial soil in Yangtze River estuary"* **Science and Engineering of Composite Materials *28***: 169–179. DOI: 10.1515/secm-2021-0016.

[10] P. Kulkarni and J. Mandal, (2022) *"Evaluation of strength characteristics of soil stabilized with nano zinc oxide—cement mixes for low volume road applications"* **International Journal of Geosynthetics and Ground Engineering *8***: 7. DOI: 10.1007/s40891-021-00346-y.

[11] A. J. Choobbasti, M. A. Samakoosh, and S. S. Kutanaei, (2019) *"Mechanical properties soil stabilized with nano calcium carbonate and reinforced with carpet waste fibers"* **Construction and Building Materials *211***: 1094–1104. DOI: 10.1016/j.conbuildmat.2019.03.306.

[12] M.-Z. Guo, T.-C. Ling, and C. S. Poon, (2017) *"Photocatalytic NOX degradation of concrete surface layers intermixed and spray-coated with nano-TiO2: Influence of experimental factors"* **Cement and Concrete Composites *83***: 279–289. DOI: 10.1016/j.cemconcomp.2017.07.022.

[13] H. Zoriyeh, S. Erdem, E. Gurbuz, and I. Bozbey, (2020) *"Nano-clay modified high plasticity soil as a building material: Micro-structure linked engineering properties and 3D digital crack analysis"* **Journal of Building Engineering *27***: 101005. DOI: 10.1016/j.jobe.2019.101005.

[14] F. Ochoa-Cornejo, A. Bobet, C. Johnston, M. Santagata, and J. V. Sinfield, (2020) *"Dynamic properties of a sand-nanoclay composite"* **Geotechnique *70***: 210–225. DOI: 10.1680/jgeot.18.P.017.

[15] N. Kananizadeh, T. Ebadi, S. A. Khoshniat, and S. E. Mousavirizi, (2011) *"The positive effects of nanoclay on the hydraulic conductivity of compacted Kahrizak clay permeated with landfill leachate"* **Clean – Soil Air Water *39***: 605–611. DOI: 10.1002/clen.201000298.

[16] N. Abbasi, A. Farjad, and S. Sepehri, (2018) *"The use of nanoclay particles for stabilization of dispersive clayey soils"* **Geotechnical and Geological Engineering *36***: 327–335. DOI: 10.1007/s10706-017-0330-9.

[17] D. Yang, X. Zhuang, X. Li, and J. He, (2025) *"Effects of lignin on the dynamic characteristics and mechanisms of silty soil"* **International Journal of Geomechanics *25***: 04025099. DOI: 10.1061/IJGNAI.GMENG-10988.

[18] X. Zhuang, X. Li, D. Yang, and B. Zhang, (2024) *"Experimental study on dynamic characteristics of xanthan gum modified silt under cyclic loading"* **Journal of Railway Science and Engineering *21***: 4532–4542. DOI: 10.19713/j.cnki.43-1423/u.T20240173.

[19] Z. Li. *"Study on the vertical load transmission through the track structure and the characteristics of subgrade dynamic stresses"*. (phdthesis). Beijing, China: China Academy of Railway Sciences, 2000. URL: https://kns.cnki.net.

[20] Y. Liu. *"Performance analysis and optimization of C70E general gondola car body"*. (mathesis). Dalian, China: Dalian Jiaotong University, 2019. DOI: 10.26990/d.cnki.gsltc.2019.000274.

[21] B. Huang, H. Ding, and Y. Chen, (2011) *"Simulation of high-speed train load by dynamic triaxial tests"* **Chinese Journal of Geotechnical Engineering *33***: 195–202. URL: https://kns.cnki.net.

[22] D. Yang, X. Zhuang, G. Tao, X. Li, and J. Fang, (2025) *"Cumulative plastic strain and shakedown analysis in loess subgrades under intermittent loads"* **Soil Dynamics and Earthquake Engineering *190***: 109224. DOI: 10.1016/j.soildyn.2025.109224.

[23] Y. Qian and G. De Schutter, (2018) *"Enhancing thixotropy of fresh cement pastes with nanoclay in presence of polycarboxylate ether superplasticizer (PCE)"* **Cement and Concrete Research *111***: 15–22. DOI: 10.1016/j.cemconres.2018.06.013.

[24] S. Pongsivasathit, S. Horpibulsuk, and S. Piyaphipat, (2022) *"Assessment of mechanical properties of cement stabilized soils"* **Case Studies in Construction Materials *16***: e00903. DOI: 10.1016/j.cscm.2019.e00301.

[25] V. Sivakumar, J. Kodikara, R. O'hagan, D. Hughes, P. Cairns, and J. D. McKinley, (2013) *"Effects of confining pressure and water content on performance of unsaturated compacted clay under repeated loading"* **Geotechnique *63***: 628–640. DOI: 10.1680/geot.10.P.103.

[26] K. Mog and P. Anbazhagan, (2022) *"Evaluation of the damping ratio of soils in a resonant column using different methods"* **Soils and Foundations *62***: 101091. DOI: 10.1016/j.sandf.2021.101091.